Cell

An Extensive MicroRNA-Mediated Network of RNA-RNA Interactions Regulates Established Oncogenic Pathways in Glioblastoma

Pavel Sumazin,[1,2,8] Xuerui Yang,[1,2,8] Hua-Sheng Chiu,[1,2,3,8] Wei-Jen Chung,[1,2,3] Archana Iyer,[1] David Llobet-Navas,[6,7] Presha Rajbhandari,[1] Mukesh Bansal,[1,2] Paolo Guarnieri,[1,2] Jose Silva,[4,6,7] and Andrea Califano[1,2,3,5,6,7,*]
[1]Columbia Initiative in Systems Biology
[2]Center for Computational Biology and Bioinformatics
[3]Department of Biomedical Informatics
[4]Department of Pathology and Cell Biology
[5]Department of Biochemistry and Molecular Biophysics
[6]Institute for Cancer Genetics
[7]Herbert Irving Comprehensive Cancer Center
Columbia University, New York, NY 10032, USA
[8]These authors contributed equally to this work
*Correspondence: califano@c2b2.columbia.edu
DOI 10.1016/j.cell.2011.09.041

SUMMARY

By analyzing gene expression data in glioblastoma in combination with matched microRNA profiles, we have uncovered a posttranscriptional regulation layer of surprising magnitude, comprising more than 248,000 microRNA (miR)-mediated interactions. These include ~7,000 genes whose transcripts act as miR "sponges" and 148 genes that act through alternative, nonsponge interactions. Biochemical analyses in cell lines confirmed that this network regulates established drivers of tumor initiation and subtype implementation, including *PTEN*, *PDGFRA*, *RB1*, *VEGFA*, *STAT3*, and *RUNX1*, suggesting that these interactions mediate crosstalk between canonical oncogenic pathways. siRNA silencing of 13 miR-mediated *PTEN* regulators, whose locus deletions are predictive of *PTEN* expression variability, was sufficient to downregulate *PTEN* in a 3′UTR-dependent manner and to increase tumor cell growth rates. Thus, miR-mediated interactions provide a mechanistic, experimentally validated rationale for the loss of *PTEN* expression in a large number of glioma samples with an intact *PTEN* locus.

INTRODUCTION

Dysregulation of physiologic microRNA (miR) activity has been shown to play an important role in tumor initiation and progression, including gliomagenesis (Gabriely et al., 2011; Godlewski et al., 2008; Kim et al., 2010a, 2011; Kwak et al., 2011). Therefore, molecular species that can regulate miR activity on their target RNAs without affecting the expression of relevant mature miRs may play equally relevant roles in cancer. Yet few such modulators of miR activity have been characterized (Krol et al., 2010; Poliseno et al., 2010), and both the extent and relevance of their role in controlling normal cell physiology and pathogenesis are poorly understood.

By analyzing a large set of sample-matched gene and miR expression profiles from The Cancer Genome Atlas (TCGA), we show here that the regulation of target genes by modulators of miR activity is surprisingly extensive in human glioma and that it affects genes with an established role in gliomagenesis and tumor subtype implementation. Specifically, we study two types of miR activity modulators with distinct molecular mechanisms (Figures 1A and 1B). Sponge modulators include both messenger RNAs (mRNAs) and noncoding RNAs, which share miR-binding sites with other RNAs. Thus, these modulators act as miR sponges, or competitive endogenous RNA (ceRNA), via an established titration mechanism (Arvey et al., 2010; Ebert et al., 2007; Poliseno et al., 2010). Depending on their expression levels and on the total number of functional miR-binding sites that they share with a target, sponge modulators can decrease the number of free miR molecules available to repress other functional targets. Nonsponge modulators, on the other hand, are implemented by proteins and RNAs acting via a variety of alternative mechanisms, including activation or suppression of miRISC-mediated regulation of target RNAs (Krol et al., 2010), protection from miR degradation (Chatterjee et al., 2011), or prevention of miRs from binding their targets (Eiring et al., 2010). As a result, they do not necessarily share miR-binding sites with their modulated targets. Established sponge modulators include *VCAN* (Lee et al., 2010), *PTENP1* (Poliseno et al., 2010), and *CD44* (Jeyapalan et al., 2011), and nonsponge modulators include miRISC core components, such as the members of the *AGO* and *TNRC6* families (Krol et al., 2010). Notably, genetic alterations at the *PTENP1*, *AGO2*, and *TNRC6A* loci have all been implicated in tumorigenesis (Kim et al., 2010b; Poliseno et al., 2010; Zhou et al., 2010).

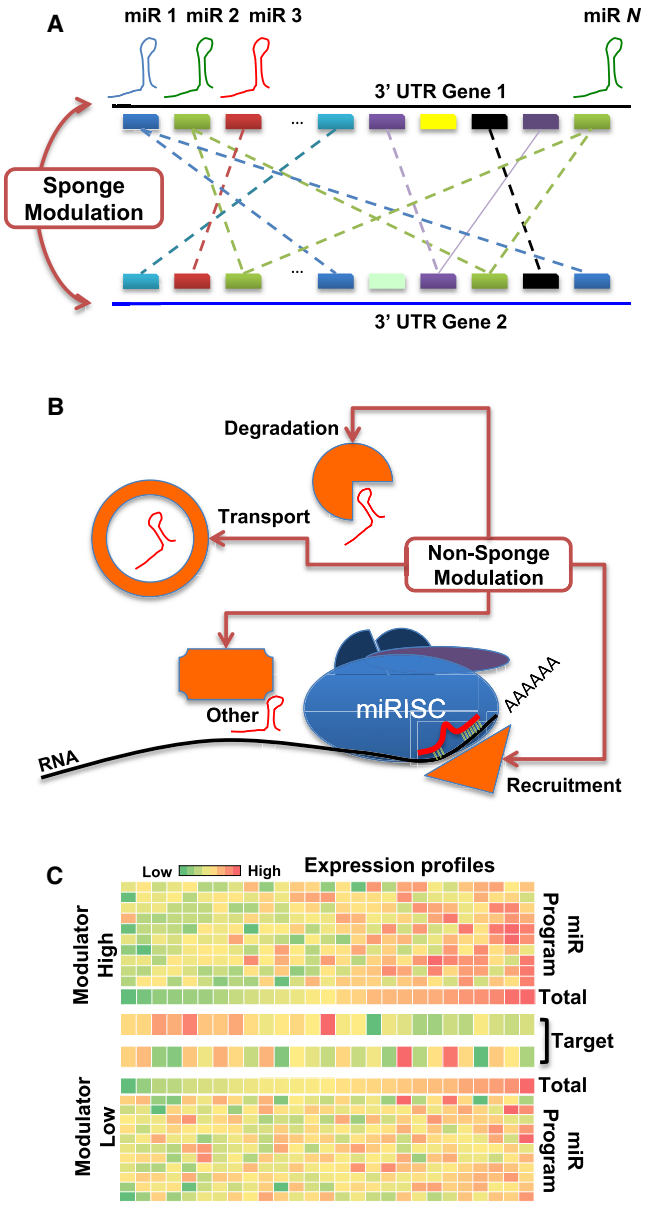

Figure 1. MiR Activity Modulators

MiR activity modulation may be implemented by several distinct mechanisms. We consider competition by RNAs for common miR programs (sponge effect) separately from other mechanisms, such as those driven by protein-protein or protein-miR interactions.

(A) RNAs modulate each other through their common miR regulatory program. Up/down changes to the expression of one RNA perturb the relative abundance of functioning miRs that target both RNAs, leading to a corresponding up/downregulation of the second RNA.

(B) Nonsponge modulators regulate miR activity by assisting or inhibiting components of the miR-mediated posttranscriptional regulatory apparatus. These regulators may help or prevent recruitment of miRISC to the target RNA or affect target degradation and transport.

(C) To identify candidate modulators, we sought out instances in which the correlation between the total expression of a miR program and its target is dependent on the expression of a candidate modulator. This image visualizes a simplification of the process. The top heatmap shows expression of miRs in a program (rows) across all samples (columns) in which the modulator expression is high, with the bottom line showing the total expression of the miR program in the sample. Samples are sorted low to high based on miR program expression. Below that is the expression of the target of the miR program. The top heatmap shows strong inverse correlation between miR-program expression and target expression, consistent with an active miR program. The bottom heatmap shows the same data but this time for samples in which modulator expression is low. Here, the negative correlation between miR program expression and target expression is reduced, which is indicative of a suppressed miR program.

To evaluate both the range and potential tumorigenic role of this class of miR-mediated interactions, we present a new multivariate analysis method called Hermes. Hermes systematically infers candidate modulators of miR activity from large collections of genome-wide expression profiles of both genes and miRs from the same tumor samples. Hermes extends the functionality of the modulator inference by network dynamics (MINDy) algorithm, which uses measurements from information theory to identify genes that modulate transcription factor activity via posttranslational modifications. MINDy has been used to infer posttranslational modulators of the MYC transcription factor in human B cells (Wang et al., 2009b), to infer signaling modulators of all transcription factors in human B cells (Wang et al., 2009a), and to identify the ubiquitin-conjugating ligase HUWE1 as a modulator of N-MYC turnover in neural stem cells (Zhao et al., 2009).

In essence, MINDy and Hermes make inferences by estimating two quantities from information theory: the mutual information (MI) and conditional mutual information (CMI). The MI quantifies how much one variable informs about another variable (i.e., high MI between two variables implies that knowledge about the first variable is predictive of state of the second variable). The CMI calculates the expected value of MI of two variables given the third variable. Specifically, given a modulator (M), a regulator (R), and a regulated target (T), the algorithms dissect the regulatory dependency of these three components by studying the difference between the CMI of the regulator's expression level and the target's expression level (conditional on the expression level of the modulator) and the MI of the regulator and target expressions, $\Delta I = I[R;T|M] - I[R;T]$ (Wang et al., 2006). These quantities and their associated statistical significance can be computed from large collections of gene expression profiles (>250 samples) using a variety of estimators for MI and CMI (Wang et al., 2006), i.e., computational tools that can quantitatively estimate their values.

Hermes expands the MINDy information theoretic framework to identify candidate genes that modulate miR activity (i.e., modulators), whose availability *M* affects the relationship between the expression of miRs targeting a gene T and its expression profile, *T*. We use the term "miR program" to indicate a set of miRs targeting a gene and the term "common miR program" to indicate the intersection between the miR programs of two distinct genes. Analysis of Hermes-inferred sponge and nonsponge interactions in TCGA glioblastoma data revealed a regulatory network of previously unsuspected size. Experimental validation of 29 such interactions (26 sponge and 3 nonsponge), of which only 3 failed to validate, suggested that Hermes has a low false positive rate and showed that its

predicted interactions participate collectively in regulation of key drivers of gliomagenesis and tumor subtype, that these interactions mediate crosstalk between independent pathways, and that they affect cell pathophysiology.

RESULTS

Whereas MINDy considers one candidate modulator/regulator/target triplet at a time, Hermes integrates the analysis across all miRs in the common miR program of two genes (sponge interactions) or in the miR program of a target gene (nonsponge interactions) using Fisher's method (Fisher, 1925). Specific technical details of the analysis are provided in the Experimental Procedures. The cartoon example of Figure 1C illustrates the type of interaction that Hermes can help to dissect. Here, the increase in expression of the modulator gene is associated with a corresponding increase in mutual information between the expression of several miRs and the expression of their common target.

In principle, one could evaluate all possible modulator/miR/target triplets and then select statistically significant ones that share the same modulator and target via different miRs. Though this would avoid having to select relevant miR programs a priori, it would also entail evaluating a huge number of triplets ($\sim 4.0 \times 10^{11}$), which is computationally prohibitive and will effectively prevent the discovery of many interactions due to excessive multiple hypothesis testing correction. Similar to MINDy, which addresses this problem by testing only triplets for experimentally validated or computationally inferred transcription factor-target interactions, we use a new miR target discovery algorithm, Cupid, which is specifically tailored to the identification of miR programs, to reduce the number of statistical tests performed by Hermes (see Experimental Procedures). Specifically, for sponge modulators, Hermes considers only modulator-target pairs (*M*, *T*) sharing a statistically significant number of miRs in their Cupid-inferred common miR programs. In addition, Hermes assumes that sponge interactions are symmetric and thus jointly evaluates the statistical significance of both *M* as a miR program-mediated modulator of *T* and *T* as a miR program-mediated regulator of *M* by combining p values using Fisher's method (Fisher, 1925). Indeed, even though miR binding and regulatory kinetics may differ in the two targets, most sponge-mediated interactions should still exhibit symmetric behavior. This is because, when averaged over the multiple miRs in their common miR program, the differences in the number of individual miR-binding sites and their regulatory kinetics should average out. As shown in Experimental Procedures, symmetry analysis confirmed that only a very small fraction of candidate sponge interactions with strictly asymmetric supporting evidence is missed by Hermes (<0.02%).

Conversely, nonsponge regulatory interactions are asymmetric by definition, as the modulator acts via alternative protein-protein or protein-RNA interaction mechanisms. Thus, they can be identified by selecting candidate (*M*, *T*) pairs with an empty or nonstatistically significant common miR program. Furthermore, because nonsponge interactions may be mediated by a single miR, rather than by a substantial miR program, use of a miR prediction algorithm may introduce too many false positive interactions. To reduce false positive predictions for nonsponge interactions, we restricted Hermes analysis to (*M*, *miR*, *T*) triplets with an experimentally validated miR-target regulatory interaction.

The miR Program-Mediated Regulatory Network

The statistical significance of $\Delta I = I[miR;T|M] - I[miR;T]$ can be effectively estimated from a large number of samples (>250) using a variety of CMI estimators (Wang et al., 2009b), provided that matched miR and gene expression profiles are available for the same samples. The Cancer Genome Atlas (TCGA) data sets are thus ideally suited for this analysis, as they are among only a handful satisfying these requirements. For this analysis, we used a publicly available set of 262 matched gene (both mRNA and noncoding RNA) and miR expression profiles from glioblastoma biopsies (TCGA, 2008). When used in a genome-wide fashion on this data set, Hermes identified nearly 7,000 sponge modulators participating in ~248,000 pairwise miR program-mediated (RNA-RNA) interactions at a highly conservative false discovery rate (FDR $< 1 \times 10^{-4}$). These interactions are summarized in Figure 2A and are enumerated in Data S1 available online. In addition, Hermes identified 148 nonsponge modulators participating in 169 miR program-mediated regulatory (mPR) interactions with more than 100 genes (Data S1), including many established oncogenes and tumor suppressors, such as *PTEN*, *RUNX1*, *TP63*, *VEGFA*, *EGFR*, *MYC*, and *NOTCH1*, among others. For these, the sponge mechanism is excluded because modulator and target have no common miR regulators. Thus, their mechanism is likely mediated by protein-protein and protein-RNA interactions. Together, sponge- and nonsponge-mediated interactions constitute a large and previously uncharacterized mPR network.

Globally, the sponge-mediated component of the mPR network presents roughly the same size and scale-free structure of typical transcriptional regulatory networks (Maslov and Sneppen, 2002). For instance, ARACNe-based reverse engineering of transcriptional interactions in glioblastoma dissected ~150,000 distinct TF-target interactions (Carro et al., 2010), compared to ~248,000 mPR interactions inferred by Hermes. We modeled the network graphically, with RNAs represented as nodes and their sponge-mediated mPR interactions as undirected edges (Figure 2A). Because inferred sponge interactions are symmetric, RNAs in this network both regulate and are regulated by their neighbor RNAs. However, mPR interactions sharing a common RNA are not necessarily mediated by the same miR program. Common miR programs supporting mPR network interactions include 18 miRs on average and up to a maximum of 153 miRs (Data S1). This suggests that, on average, sponge modulation effects associated with each individual miR in a common program may be negligible compared to the global effect of the entire program.

The mPR network contains many highly interconnected (i.e., dense) structures, i.e., N gene subgraphs, with a number of internal edges approximating the theoretical maximum of $N_{max} = N(N-1)/2$. Indeed, the largest dense glioma mPR structure is a 564 node, 111 core subgraph (Barrat et al., 2008), i.e., a structure in which each RNA is directly linked to at least 111 of the other 563 RNAs (Data S1). RNAs in these dense subgraphs are strongly coexpressed, as each RNA tracks the average

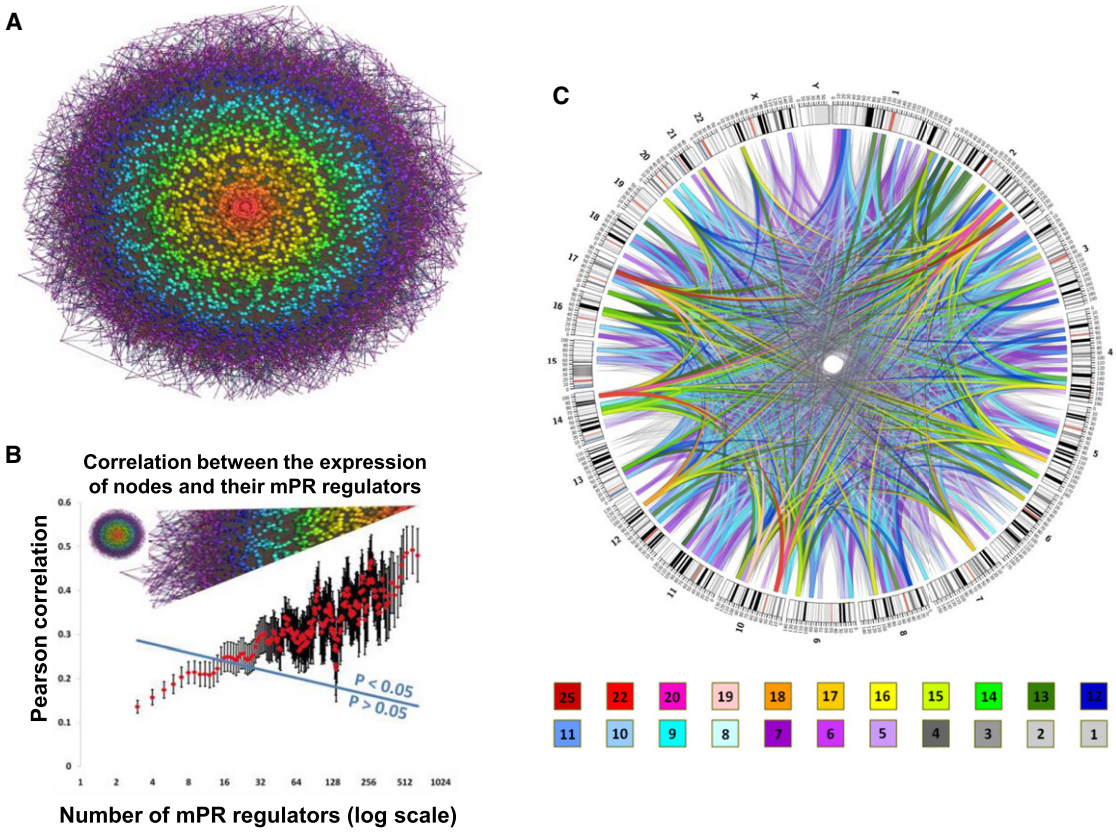

Figure 2. The mPR network

(A) Genome-wide inference of sponge modulators identified a miR program-mediated posttranscriptional regulatory (mPR) network including ~248,000 interactions. Its graphic visualization uses nodes to represent individual RNAs and edges to represent miR program-mediated RNA-RNA interactions. Nodes near the center of the graph are contained within more tightly regulated, dense subgraphs, with the densest 564 node subgraph shown in red at the center of the network. The network is scale free, and the color bands, which include nodes with similar connectivity, have a size that increases exponentially with the distance from the center.

(B) The correlation between expression of RNAs and the total expression of their mPR regulators (i.e., all of its mPR neighbors) is plotted as a function of the number of its mPR regulators; genes at the center of the mPR network are regulated by hundreds of mPR regulators and are significantly correlated with their total expression. Values above the blue line are statistically significant at $p < 0.05$.

(C) The 564 node mPR subgraph facilitates interactions between the loci of distal genes. Colors designate the number of gene-to-gene edges connecting each 10 Mb chromosomal region.

See also Figure S1 and Data S1.

expression of the other subgraph members that it is connected to. Densest subgraph RNAs and their interactions are shown in red, near the center of Figure 2A. Conversely, subgraphs near the edge of the figure, which are shown in purple, are sparser, and their members are less coexpressed. Nodes in the network are clustered according to their subgraph connectivity, and each node is depicted with a color representing the size of the subgraph that contains it. The mPR network is scale free (see Extended Experimental Procedures). Thus, the number of same-color nodes in a band increases exponentially with their distance from the center (Figure 2A).

The overall regulatory effect on a node depends on many variables, including the number of its mPR neighbors, the size of the miR programs that mediate its interactions, and the individual kinetics of the individual miR-target interactions that it shares with its neighbors. In general, however, nodes in larger highly connected subgraphs will have more neighbors and will thus be more strongly regulated by their mPR interactions. Indeed, coexpression of RNAs in a subgraph increases exponentially with the subgraph size, as shown in Figure 2B.

Analysis of the mPR network shows that mPR interactions participate in distal regulation between genes within and across chromosomes (see Figure 2C by Circos) (Krzywinski et al., 2009). In addition, analysis of KEGG pathway genes (Kanehisa and Goto, 2000) targeted by mPR interactions shows that this interaction layer mediates crosstalk between numerous pathways (see Figure S1 and Data S1).

PTEN Expression Is Regulated by mPR Interactions

PTEN downregulation is a hallmark of gliomagenesis, and its locus has been identified as one of the most frequently altered in glioblastoma (Verhaak et al., 2010). Though homozygous deletions at the *PTEN* locus are rare, appearing in less than 2% of glioblastoma samples, *PTEN* is haploinsufficient, and even

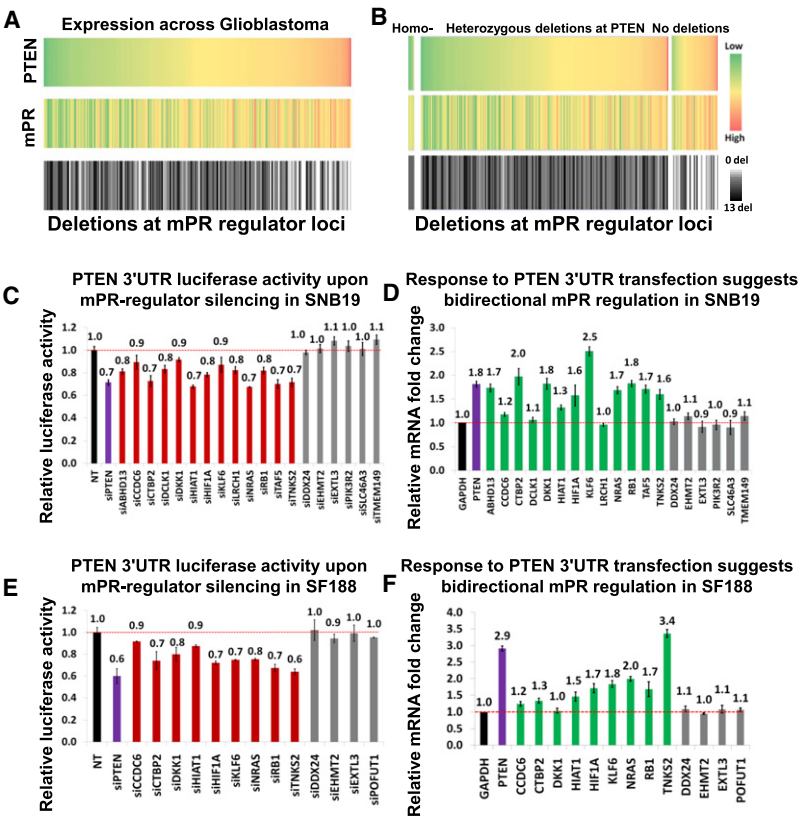

Figure 3. *PTEN* Expression Is Correlated with the Expression of Its mPR Regulators

(A) PTEN is targeted by > 500 mPR regulators, and its expression is correlated with both their total gene expression and with deletions at their loci; in aggregate, 97% of the TCGA glioma tumors have at least one deletion in a PTEN mPR regulator locus. We selected 13 mPR regulators of PTEN with enriched locus deletions in *PTEN* intact tumors. As shown, their collective deletions and total expression are both significantly correlated with *PTEN* expression ($p_D < 2 \times 10^{-10}$ and $p_E < 5 \times 10^{-23}$, respectively).

(B) Surprisingly, the correlation between *PTEN* and the aggregate expression across the 13 genes is significant in both samples with an intact *PTEN* locus and samples with heterozygous deletions ($r_D = 0.40$, $p_D < 10^{-9}$ and $r_{WT} = 0.46$, $p_{WT} < 4 \times 10^{-4}$ by Pearson correlation, respectively). The range of *PTEN* expression in *PTEN* heterozygously deleted samples and in samples with an intact *PTEN* locus was virtually the same.

(C) Individual siRNA-mediated silencing of 13 PTEN mPR regulators reduced *PTEN* 3′UTR luciferase activity in SNB19 cells at 24 hr. Negative control targets (in gray) were unaffected.

(D) Ectopic expression of *PTEN* 3′UTR increased expression of 13 PTEN mPR regulators in SNB19 cells at 24 hr, compared to empty vector. Negative control targets (in gray) were unaffected.

(E and F) Results in SNB19 were replicated in SNF188 cells for genes that are expressed in this cell line. Fold change was measured by qRT-PCR.

Data are represented as mean ± SEM. See also Figure S2 and Data S1.

moderate *PTEN* downregulation at the protein level, such as that resulting from loss of a single allele, may be tumorigenic. Surprisingly, however, the range of *PTEN* expression in heterozygously deleted samples is comparable to its range of expression in samples in which its locus is intact (Figures 3A and 3B), suggesting that its expression may be tightly regulated and that a variety of additional mechanisms may contribute to its downregulation in tumors. PTEN regulation by miRs is well established. In glioblastoma, for instance, amplifications at the miR-26a locus have been implicated with downregulation of PTEN (Kim et al., 2010a). Interestingly, *PTEN* is one of the genes in the densest 111 core subgraph, with a total of 534 interactions in the mPR network (Data S1), suggesting that its expression is strongly regulated by sponge effect. Indeed, not only do > 80% of the tumors with an intact *PTEN* locus have deletions in at least one of the PTEN mPR regulator loci (44/53 as of March, 2011). But the total number of such deletions in each sample is highly predictive of *PTEN* expression ($p < 10^{-4}$ by permutation testing) (see Figure 3B). Interestingly, these deletions are more predictive of *PTEN* expression in *PTEN* wild-type tumors than in tumors with *PTEN* heterozygous deletions, suggesting that mPR regulators may account for missing *PTEN* genetic variability in glioblastoma.

We focused on a subset of 13 *PTEN* mPR regulators that are expressed in the glioblastoma cell line SNB19 and whose loci are enriched for deletions in tumors with an intact *PTEN* locus (25/53); interestingly, these 25 tumors include all of the 8/53 *PTEN* intact tumors with amplification at the miR-26a. The total number of deletions at these 13 gene loci, as well as their total mRNA expression, was found to be highly predictive of *PTEN* expression not only in *PTEN* intact samples, but also across all 262 tumors tested in our analysis (Figures 3A and 3B and Data S1; $p_{Del} < 2 \times 10^{-10}$ and $p_E < 5 \times 10^{-23}$ by Pearson correlation analysis, respectively). Correlation between the genetics and genomics of *PTEN* mPR regulators and *PTEN*'s mRNA expression suggests that deletions at *PTEN* mPR loci may collectively represent a key contribution to loss of *PTEN* expression in glioblastoma. In addition, *PTEN* is not the only gene whose expression may be regulated by deletions at the loci of its mPR regulators. In total, glioblastoma expression profiles of 292 genes, including many known drivers of tumorigenesis and tumor subtypes such as *RUNX1*, *PTPRN*, *FGFR3*, *TGFBR2*, and *DICER1*, were significantly correlated ($p < 0.001$) with deletions at the loci of their mPR regulators (Data S1). Strikingly, the expression profiles of more than half of these genes had stronger correlation with deletions at the loci of their mPR regulators than with deletions at their own loci.

To confirm functional mPR-based *PTEN* regulation by these 13 mPR regulators, we performed siRNA-mediated silencing of each gene in SNB19 cells (see Figure S2 for silencing efficiency estimates) and measured the effect on *PTEN* using a *PTEN* 3′UTR luciferase reporter assay. Silencing of 11 of the 13 modulators in SNB19 leads to a significant ($p < 0.01$) reduction in *PTEN* luciferase activity, compared to negative controls (Figure 3C). To

further validate that this regulatory mechanism is symmetric in nature, thus allowing *PTEN* expression to modulate the same 13 genes, we transfected SNB19 cells with *PTEN* 3′UTR and measured the effects on modulator expression (Figure 3D). This also addressed the potential issue that siRNA-mediated silencing may perturb endogenous miRs, possibly affecting the results displayed in Figure 3C. Upregulation of 10 of the 13 modulators was significant ($p < 0.01$). Overall, 13/13 tested interactions were positive either in siRNA silencing or in 3′UTR expression assays. To ensure that the effects are not cell line specific, we repeated the two experiments in the glioblastoma cell line SF188, using the subset of genes that were expressed in this cell line (9/13) (Figures 3E and 3F). Results in SF188 confirmed the SNB19 results: indeed, silencing nine of the nine modulators lead to a significant reduction in *PTEN* luciferase activity, and transfection with *PTEN* 3′UTR upregulated seven of the nine modulators. Taken in aggregate, the cumulative Fisher's p value across all of the experiments is effectively below machine precision ($p < 10^{-221}$ based on an analytical estimate).

To show that these effects are specific to mPR regulators, six negative control genes were selected randomly among those that (1) are not *PTEN* neighbors in the mPR network, (2) have variable length UTRs, and (3) show a variety of correlation patterns with *PTEN*'s mRNA expression (positively correlated, negatively correlated, and uncorrelated). Randomly selected genes include *TMEM149* (30 base 3′UTR), *POFUT1* (4003 base 3′UTR), *DDX24* (269 base 3′UTR), *SLC46A3* (1416 base 3′UTR), *EXTL3* (2819 base 3′UTR), *PIK3R2* (1239 base 3′UTR), and *EHMT2* (324 base 3′UTR). Of these, expression profiles of *DDX24* and *SLC46A3* are significantly positively correlated with that of *PTEN*, whereas *POFUT1* expression is significantly anticorrelated with *PTEN* expression. All of these genes except for *POFUT1* were highly expressed and could be silenced in SNB19 cells, whereas only *DDX24*, *EHMT2*, *EXTL3*, and *POFUT1* were expressed and could be silenced in SF188 cells. As predicted, *PTEN* 3′UTR luciferase activity was unchanged after silencing these genes in both cell lines (see Figures 3C and 3E). Furthermore, their mRNA expression was not significantly affected following transfection with *PTEN* 3′UTR (see Figures 3D and 3F). As an additional negative control, transfection of both SNB19 and SF188 cells with *PIK3R2* 3′UTR, which is not inferred as a PTEN or an RB1 regulator, failed to affect PTEN, RB1, and the vast majority of their selected mPR regulators (see Figure S3A). Finally, transfection with *PTEN* cDNA, which lacks a 3′UTR region, failed to alter the expression of tested PTEN mPR regulators (Figure S3B). Note that the expression of these genes was affected by transfection with *PTEN* 3′UTR (Figures 3D and 3F). Taken together, these results confirm miR-mediated interactions between predicted mPR RNA pairs, including PTEN and its predicted mPR regulators, but not between these genes and other randomly selected genes (negative controls), regardless of their correlation with *PTEN* expression or the lengths of their UTRs.

Tumor Growth Is Regulated by PTEN mPR Interactions

To test whether PTEN mPR regulators may affect tumor cell growth, as previously shown for PTEN's posttranscriptional regulator *PTENP1* (Poliseno et al., 2010), we measured SNB19 and SF188 cell growth rates in response to transfection of PTEN cDNA (missing the 3′UTR) and 3′UTR, as well as to siRNA-mediated silencing of PTEN and of its Hermes-inferred mPR regulators (Figure 4). Transfection of *PTEN* 3′UTR upregulated the expression of its mPR neighbors, increased PTEN (protein) concentration, and reduced tumor cell growth rates. Conversely, siRNA-mediated silencing of 10/13 and 9/9 mPR regulators reduced *PTEN* 3′UTR-luciferase expression and significantly accelerated SNB19 and SF188 cell growth, respectively. The effect of silencing these regulators was comparable to that of siRNA-mediated PTEN silencing, and the aggregate p value for the significance of the increase in tumor cell growth computed by Fisher's method is below machine precision (i.e., $p \approx 0$).

To demonstrate that mPR regulation is not limited to the *PTEN* and its mPR neighbors but is rather a general property of the mPR network, we further tested the ability of RUNX1, a master regulator of the glioma mesenchymal subtype (Carro et al., 2010), to regulate its Hermes-predicted neighbors. Indeed, transfection with *RUNX1* 3′UTR in SNB19 cells was equally effective in upregulating four of its fives mPR neighbors (Figure S4).

Glioma Regulators Form a Dense Subgraph in the mPR Network

The mPR network may explain significant crosstalk among different regulatory compartments of the cell that are observed in perturbation experiments (Chow et al., 2011). Indeed, further investigation of the mPR network revealed that known drivers of glioma tumorigenesis and glioblastoma subtypes *RB1*, *PTEN*, *RUNX1*, *PDGFRA*, *STAT3*, and *VEGFA* (Carro et al., 2010; Parsons et al., 2008; Verhaak et al., 2010) are part of a dense subgraph of mutually mPR-interacting genes (Figure 5A). Ectopic expression of PTEN 3′UTR was effective in upregulating expression of the other genes in this subgraph, and siRNA-mediated silencing of DICER and DROSHA (necessary for miR processing) was sufficient to abrogate the effect, suggesting that these interactions are miR mediated (Figure 5B). To further confirm symmetric posttranscriptional regulation across all genes in the subgraph, we measured their response to transfection with the 3′UTRs of all other genes in the subnetwork in SNB19 cells by qRT-PCR, except for VEGFA, whose 3′UTR cloning was not successful. Results confirmed that ectopic expression of the 3′UTRs of genes in this subnetwork upregulated expression of the other genes (Figures 5B and 5C). In particular, ectopic expression of *PTEN* and *RB1* 3′UTRs led to a > 50% upregulation of both genes, suggesting significant miR-mediated crosstalk between the *PTEN* and *RB1* pathways, both implicated in gliomagenesis. Moreover, co-ectopic expression of 3′UTR pairs at 50% concentration for each UTR intensified the regulatory response (Figure 5D), suggesting that the effect of multiple mPR modulation is more than additive, as suggested by results shown in Figure 2B.

Cooperativity between some of the regulators in the subnetwork has been implicated in high-grade gliomagenesis (Chow et al., 2011), despite their distinct functions, lack of common transcriptional regulation, and large genomic distances. In

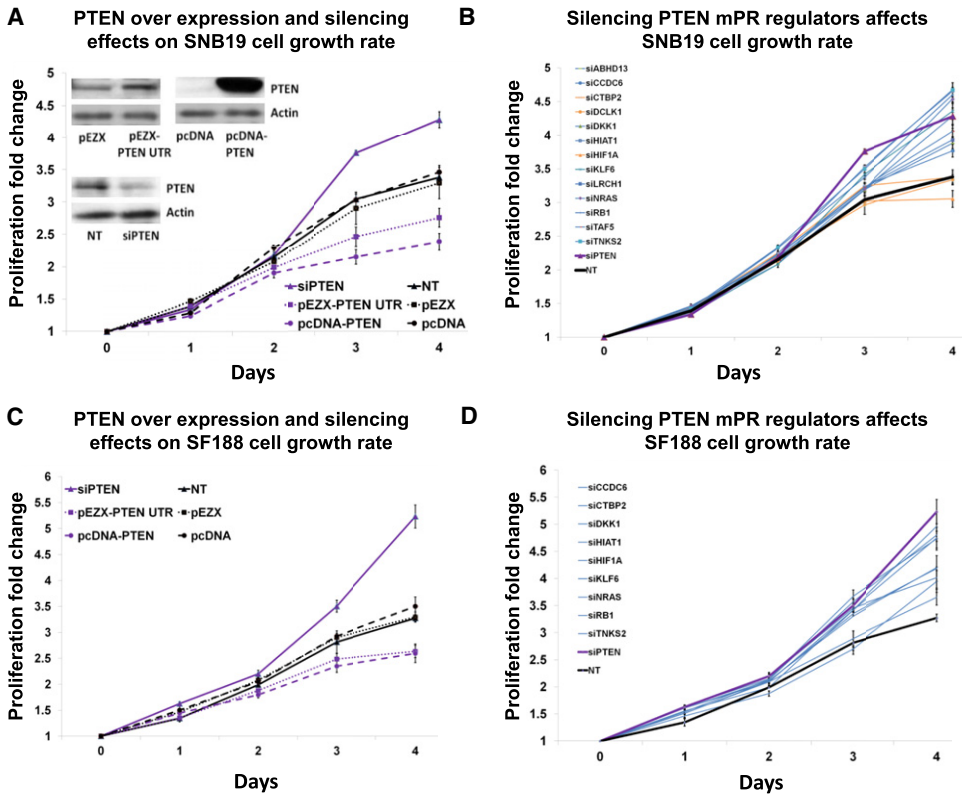

Figure 4. Silencing of PTEN mPR Regulators Accelerates Tumor Cell Growth

(A) Cell proliferation assays were performed at 24 hr intervals, up to 4 days, following siRNA-mediated PTEN silencing, *PTEN* cDNA ectopic expression, and *PTEN* 3′UTR ectopic expression. Protein levels of *PTEN* were assessed by western blotting at day 1.

(B) Cell proliferation assays were performed at 24 hr intervals, up to 4 days, following siRNA-mediated silencing of 13 PTEN mPR regulators. Nontarget (NT) siRNA was used as a control.

(C and D) Results in SNB19 were replicated in SNF188 cells for genes that are expressed in this cell line.

Data are represented as mean ± SEM. See also Figure S3.

particular, the loci of tumor suppressors PTEN and RB1 are frequently deleted in high-grade glioma (*PTEN*, 80%; RB1, 33%; *PTEN*+RB1, 85%). Analysis of 3′UTR luciferase activity of five of the six genes (Figure 5A), following siRNA-mediated silencing of PTEN and RB1, confirmed the presence of the predicted regulatory interactions (Figure 6). Thus, our results suggest that PTEN and RB1 regulate one another posttranscriptionally through 32 miRs in a common program (Data S1) and that their availability significantly affects expression of other genes in the same subgraph, with an established role in gliomagenesis. Overall, six of eight predicted interactions were confirmed by these assays. Additionally, of 11 experimentally validated interactions between these genes, six were predicted, suggesting a false negative rate of ~45%. Full analysis of mPR interactions between genes in selected KEGG pathways (Kanehisa and Goto, 2000) is presented in Figure S1 and enumerated in Data S1.

Nonsponge-Related miR Activity Modulation

As discussed, to identify nonsponge miR activity modulators, we restricted our analysis to candidate modulators of literature-validated miR-target interactions. Because prediction of individual miR targets is still inaccurate, we could not rely on the robust statistics afforded by large miR programs, as used when predicting sponge modulators. Even with this substantial limitation, Hermes could identify 148 miR activity modulators, suggesting that this number may increase substantially once a more comprehensive, high-accuracy miR target network is available. To experimentally confirm nonsponge modulator candidates inferred by our analysis, we selected three interactions, two affecting PTEN and one affecting RUNX1. These include WIPF2, as a miR-mediated regulator of RUNX1, and PALB2 and WNT7A, as miR-mediated regulators of PTEN (Figure 7A). Both PTEN and RUNX1 are known drivers of gliomagenesis (Carro et al., 2010; Verhaak et al., 2010), and genes that regulate their expression may play a role in this disease.

Upregulation of WNT7A by transfection of its cDNA sequence, which lacks both 5′ and 3′UTRs, led to 1.5-fold upregulation of PTEN or *PTEN* 3′UTR luciferase activity (Figures 7B and 7E), suggesting that, as predicted, WNT7A regulation of PTEN is miR dependent, but not sponge mediated. Silencing PALB2 led to a 1.5-fold upregulation of PTEN or *PTEN* 3′UTR luciferase activity (Figures 7C and 7E), and silencing WIPF2 led to a 3-fold upregulation of *RUNX1* expression and 2-fold upregulation of *RUNX1* 3′UTR luciferase activity (Figures 7D and 7F),

both consistent with computational predictions of miR-mediated downregulation. Consistent with miR-dependent regulation, DROSHA and DICER silencing (Figure 7G) abrogated PTEN and RUNX1 regulation by WNT7a/PALB2 and WIPF2, respectively (Figures 7E and 7F). Expression of validated miRs targeting these genes, such as mir-21 (*WNT7A*), mir-106a (*PALB2*), and mir-17-5p (*WIPF2*), were relatively unchanged (Figure S5).

DISCUSSION

Hermes Unveils an Extensive Layer of miR-Mediated Posttranscriptional Regulation

Genome-wide Hermes analysis supports the existence of a miR-mediated, posttranscriptional regulation layer of unsuspected magnitude, the mPR network, effected both by sponge and non-sponge interactions. Though the specific mechanism of sponge modulation and the potential for miR-gene interactions were previously reported (Arvey et al., 2010; Carro et al., 2010; Krol et al., 2010; Poliseno et al., 2010; Su et al., 2011), both the extent and the functional relevance of this regulatory layer were unknown. In terms of size, the mPR layer rivals transcriptional regulation, supporting regulation of thousands of RNA species and modulating crosstalk between distinct regulatory pathways. Changes in two or more mPR regulators of a target gene may have effects comparable to transcriptional regulation (i.e., >2-fold changes), as suggested by Figure 2C and as shown in Figures 5C and 5D.

The mPR network discovered here is implemented by sponge-mediated interactions that are generally symmetric in nature and in a sponge-independent fashion by multiple gene products (e.g., proteins and RNAs) that affect miR target regulation asymmetrically. Given the genome-wide nature of the algorithm used to infer nonsponge mPR regulation, elucidation of the variety of mechanisms that may support them cannot be accomplished at this stage. However, the experimentally validated existence of this class of interactions suggests a variety of mechanisms for future testing, some of which have been previously elucidated (Figure 1B). A key and potentially confusing point is that our analysis suggests that mPR sponge interactions are mediated by relatively large miR programs, including, on average, 18 and up to 153 miRs (Table S1). As a result, the effect of individual miRs is relatively negligible, and mPR regulation is unlikely to be significantly affected by modulation of individual miRs or miR-binding sites in isolation. In addition, two other articles in this issue of *Cell* (Tay et al., 2011; Karreth et al., 2011) also report the identification of a regulatory network of miR "sponges" (or competitive endogenous RNAs) in cancer, and a third article in this issue (Cesana et al., 2011) reports the discovery of a long noncoding RNA that regulates muscle differentiation via a "sponge-like" mechanism, as well.

Importantly, though we have validated a substantial set of miR-mediated PTEN modulators in multiple cell lines, this by no means constitutes a thorough validation of the entire network. Yet, out of the 29 predicted interactions that we tried to experimentally validate, including 26 sponge-mediated ones (Figures 3C–3F, 5, 6, and S4) and three nonsponge-mediated ones (Figure 7), all but six were confirmed (all but three if one considers both 3′UTR expression and siRNA-mediated silencing assays in Figures 3C and 3D). This suggests that our false positive rates are low (~10%–20%), comparing favorably with false positive rates in typical high-throughput experimental procedures. Thus, if globally validated using the experimental assays proposed in this manuscript, which is not currently feasible even using high-throughput approaches, a substantial number of the predicted interactions should be confirmed. Furthermore, we validated all of the pairwise interactions in the dense subgraph that includes *PTEN*, *STAT3*, *VEGFA*, *PDGFRA*, *RUNX1*, and *RB1*. Of the 11 that were experimentally validated, five were not predicted, suggesting a false negative rate of ~45%, which is also competitive with experimental false negative rates.

In addition, limitation of nonsponge modulator analysis strictly to literature-validated miR-target interactions suggests that, when extrapolated to the full set of miR-target interactions in a cellular context, nonsponge interactions may be far more numerous. Finally, though we focused on regulation of mRNAs through miRs that target 3′UTRs, miR-mediated regulation is not restricted to 3′UTR targeting (Chi et al., 2009; Hafner et al., 2010), and miRs are known to target noncoding RNAs (Poliseno et al., 2010), which suggests that the scope of this network needs to be further expanded.

MiR Activity Modulators Regulate Pathogenesis of Disease

It is important to note that, though individual miR-mediated interactions may be weak, their regulatory effect in combination is substantial (Figures 2B and 5D). Furthermore, their ability to affect cellular phenotype is also significant and comparable to what was previously described for *PTENP1* (Poliseno et al., 2010), whose deletion was shown to be tumorigenic in vivo. This suggests that miR-mediated interactions between genes may play an important role in disease initiation and progression when dysregulated. Indeed, analysis of large glioblastoma data sets revealed that miR-mediated PTEN regulators are highly predictive of PTEN downregulation even when the *PTEN* locus is intact and may account for a significant proportion of the missing genetic variability of the *PTEN* locus.

In this manuscript, we focused on *PTEN* as a key driver of gliomagenesis whose locus is often altered in glioblastoma samples (Verhaak et al., 2010). However, regulation by miR activity modulators is not limited to *PTEN* or to glioma. In this study, we showed that a variety of well-established drivers of tumorigenesis and tumor subtype in glioblastoma are regulated by miR activity modulators, and our computational predictions suggest that other established oncogenes and tumor suppressors are similarly regulated. Because these effects are miR mediated and miR expression is strongly cell context dependent, mPR networks are likely to be context specific, and their structure and contribution to disease initiation and progression will need to be studied independently in different contexts.

Direct Screening Methods Are Required for Systematic Prediction

Hermes, the algorithm used for the identification of miR activity modulators, presents two key advantages. First, by definition, nonsponge modulators cannot be inferred by miR target analysis. Thus, Hermes provides the only systematic computational

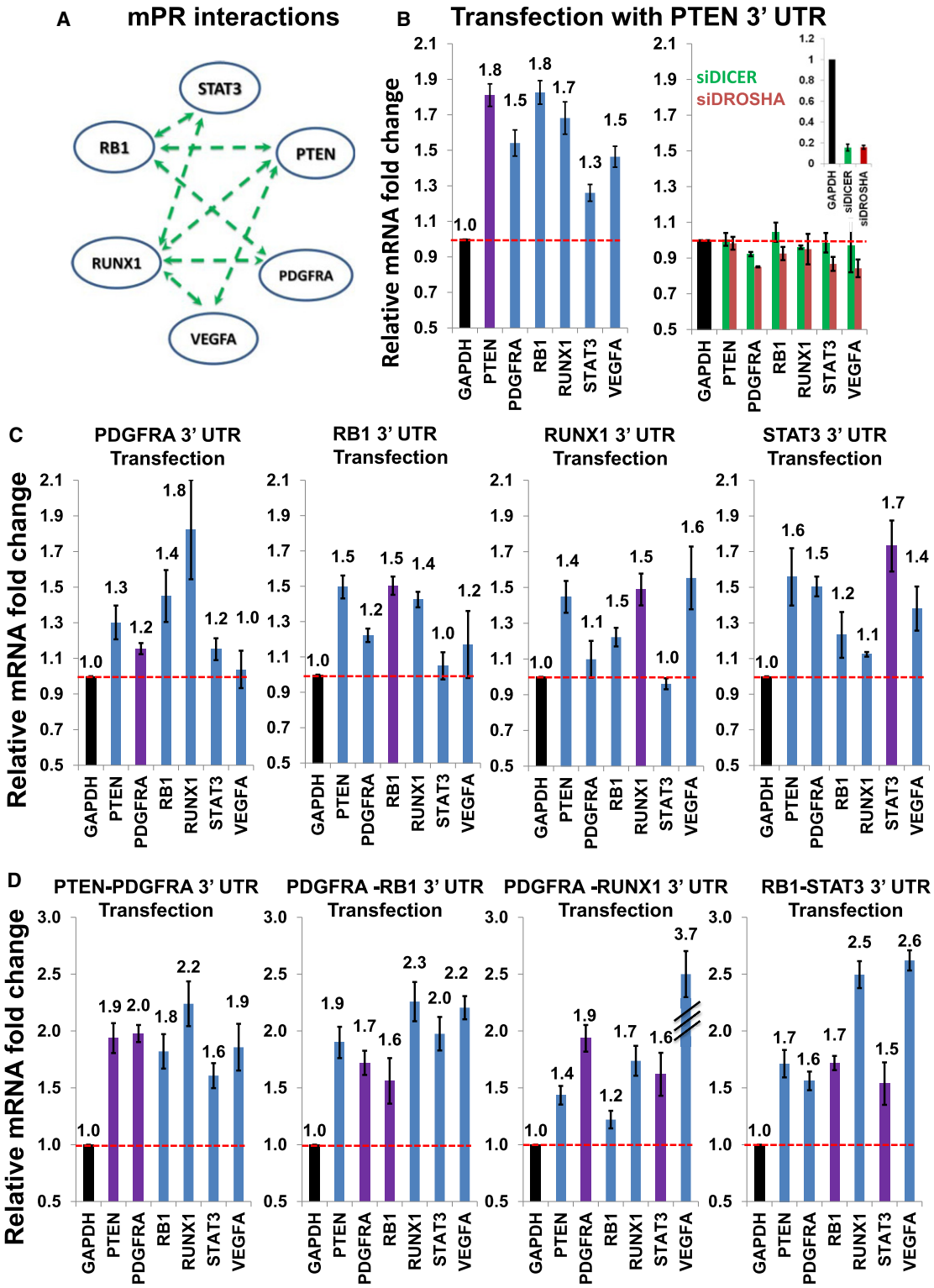

Figure 5. 3′ UTR Transfections Confirm miR-Mediated Interactions between Key Drivers of Glioma

(A) A tightly interconnected mPR network subgraph was identified, which includes established drivers of gliomagenesis. Sponge-mediated interactions inferred by Hermes are shown as dotted green lines.

(B) Gene expression fold change of *PTEN*, *PDGFRA*, *RB1*, *RUNX1*, *STAT3*, and *VEGFA* at 24 hr following ectopic expression of *PTEN* 3′UTR, compared to an empty vector, with (right) and without (left) siRNA-mediated silencing of DICER and DROSHA.

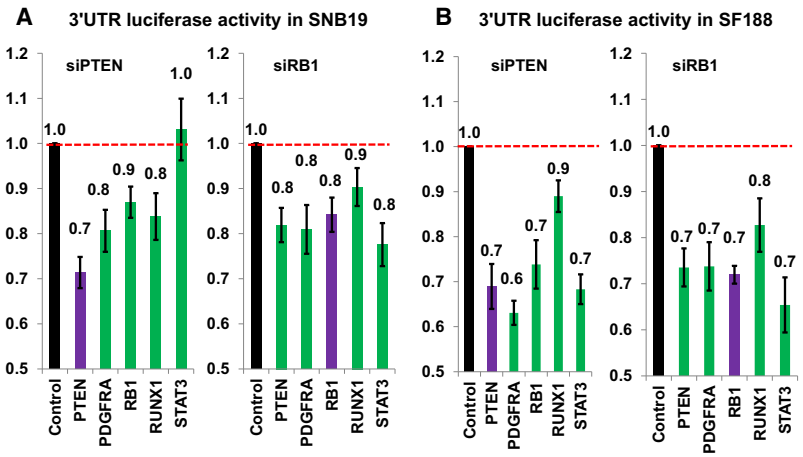

Figure 6. 3′UTR Luciferase Activity Assays Confirm miR-Mediated Interactions between Key Drivers of Glioma

(A) 3′UTR luciferase activity of *PTEN*, *PDGFRA*, *RB1*, *RUNX1*, and *STAT3* were measured in SNB19 cells at 24 hr following siRNA-mediated silencing of PTEN and RB1 compared to nontargeting siRNAs (NT5) as control (in black).

(B) Results in SNB19 were replicated in SNF188 cells. Similar to Figure 5, y axes start at 0.5.

Data are represented as mean ± SEM.

approach to determine this kind of interaction. Second, though it may be possible to infer sponge modulators by miR target analysis alone, for instance by identifying genes whose transcripts share common miR-binding sites, identification of functional miR targets is still largely inaccurate, with different methods predicting widely different interactions. Hermes circumvents this problem by first integrating evidence from multiple miRs in a common program and then by requiring direct, multivariate expression-based evidence for the predicted interaction by conditional mutual information analysis. Thus, false negative predictions by miR target prediction algorithms are much less critical than false positive predictions, as the latter dramatically reduce the statistical power of the method by increasing the number of hypotheses tested by the algorithm. On the other hand, even if miR program size is reduced by false negatives, conditional mutual information analysis can still filter false positive interactions. As a result, rather than relying on existing algorithms for miR target prediction, which still have substantial false positive rates, we implemented Cupid specifically to reduce false positive predictions even if at the expense of some false negative predictions (Extended Experimental Procedures). Indeed, Cupid predicts fewer miR-target interactions than the intersection of three established algorithms, TARGETSCAN (Lewis et al., 2005), PITA (Kertesz et al., 2007), and MIRANDA (Enright et al., 2003). However, when we replaced Cupid predictions by the intersection of the three algorithms, 25 out of 26 experimentally validated mPR interactions in this manuscript were missed. As a result, though our analysis does not suggest that Cupid may outperform other algorithms in terms of miR target identification, its specific design, aimed at minimizing false positives at the expense of false negatives, is uniquely tailored to inferring miR programs for further Hermes analysis.

Conclusions

Periodically, we are faced with the emergence of new regulatory layers, the posttranscriptional and histone modification ones being the latest additions. Every time that this happens, we discover that these layers account for a significant amount of missing genetic and epigenetic variability in the etiology of disease. As a result, as suggested by our data, it is reasonable to expect that this extensive miR-mediated interaction layer, which allows gene regulation without direct transcriptional or even posttranscriptional interactions, will also provide a number of clues to the dysregulation of key mechanisms of pathogenesis as well as to the regulation of normal cell physiology.

EXPERIMENTAL PROCEDURES

We used a miR activity modulator screening algorithm, Hermes, to identify candidate miR activity modulators by finding genes whose expression is correlated with deviations in coexpression between miR programs and their targets using conditional mutual information. We used an integrative miR target prediction algorithm, Cupid, to predict miR-target interactions and to assemble miR regulatory programs for 3′UTRs. We identified genomic alterations using snapCGH (Marioni et al., 2006). Level 3 Agilent gene and miR expression data for glioma tumors were obtained from TCGA (TCGA, 2008). The glioblastoma cell lines SNB19 and SF188 were cultured under standard conditions. Transient transfections of expression vectors were used to overexpress genes and 3′UTRs; siRNAs were used for mRNA silencing; real-time PCR, luciferase activity, western blots, and proliferation assays were performed according to standard protocols. Our methods and experimental procedures are described in detail in the Extended Experimental Procedures.

SUPPLEMENTAL INFORMATION

Supplemental Information includes Extended Experimental Procedures, five figures, and one data file and can be found with this article online at doi:10.1016/j.cell.2011.09.041.

ACKNOWLEDGMENTS

We thank James Chi-ping Chen and Mariano J. Alvarez for critical discussion and Katia Basso, Francesco Niola, Antonio Iavarone, and Anna Lasorella for

(C) Gene expression fold change of *PTEN*, *PDGFRA*, *RB1*, *RUNX1*, *STAT3*, and *VEGFA* at 24 hr following ectopic expression of *PDGFRA*, *RB1*, *RUNX1*, and *STAT3* 3′UTRs, compared to empty vector.

(D) Gene expression fold change of *PTEN*, *PDGFRA*, *RB1*, *RUNX1*, *STAT3*, and *VEGFA* at 24 hr following ectopic expression of 3′UTR pairs, including double transfections of *PTEN* and *PDGFRA*, *PDGFRA* and *RB1*, *PDGFRA* and *STAT3*, and *RB1* and *STAT3* 3′UTRs. Gene expression was assessed by qRT-PCR. To highlight the significance of the change, note that y axes start at 0.5 to better visualize the ratio between the experimental error and the change in expression. Data are represented as mean ± SEM. See also Figure S4.

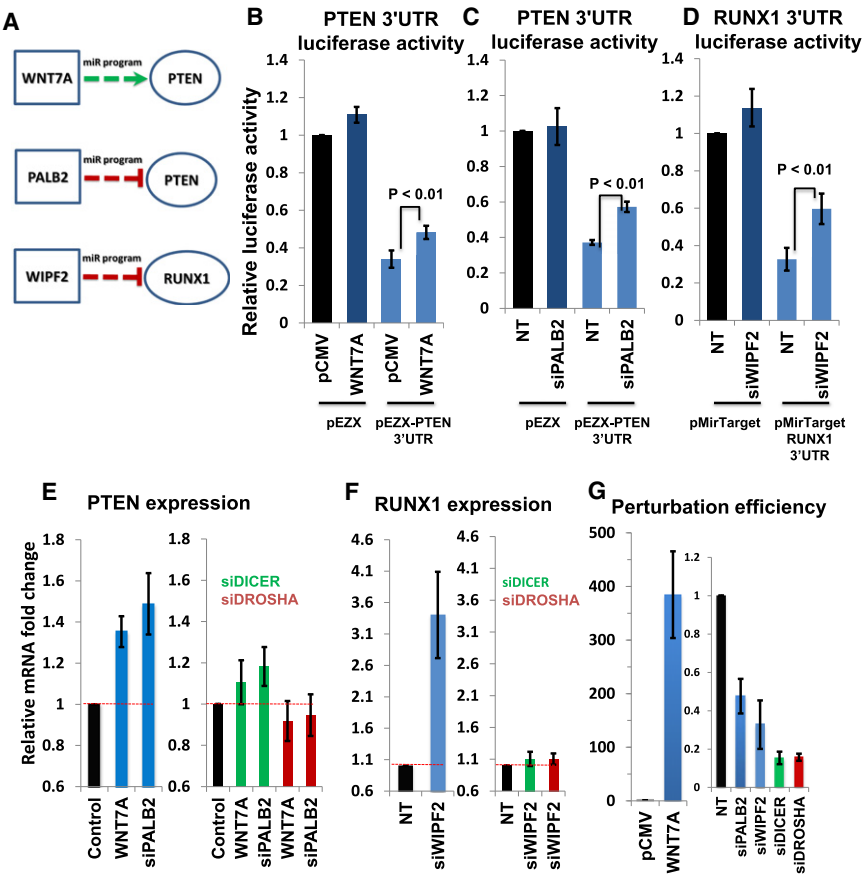

Figure 7. Validation of Nonsponge miR Activity Modulators

(A) Validated nonsponge modulators include WNT7A and PALB2 (predicted to induce miR-dependent upregulation and downregulation of PTEN, respectively) and WIPF2 (predicted to induce miR-dependent downregulation of RUNX1).

(B) *PTEN* 3′UTR luciferase activity and activity of the empty luciferase vector (pEZX) were measured at 24 hr following ectopic expression of pCMV-WNT7A or empty vector pCMV.

(C) *PTEN* 3′UTR luciferase activity and activity of the empty luciferase vector (pEZX) were measured at 24 hr following siRNA-mediated silencing of PALB2 versus nontarget siRNA.

(D) *RUNX1* 3′UTR luciferase activity (pMirTarget-*RUNX1* 3′UTR) and activity of the empty luciferase vector (pMirTarget) at 24 hr following siRNA-mediated silencing of WIPF2 and nontarget (NT5) siRNA.

(E) qRT-PCR analysis of *PTEN* gene expression fold change at 24 hr following ectopic expression of WNT7A and siRNA mediated silencing of PALB2 without (left) and with (right) siRNA-mediated silencing of DROSHA and DICER.

(F) qRT-PCR analysis of *RUNX1* gene expression fold change at 24 hr following siRNA-mediated silencing of WIPF2 without (left) and with (right) siRNA-mediated silencing of DROSHA and DICER.

(G) Efficiency of WNT7A ectopic expression and of siRNA-mediated silencing of PALB2, WIPF2, DICER, and DROSHA, measured by qRT-PCR analysis.

Data are represented as mean ± SEM. See also Figure S5.

support and suggestions. We would also like to acknowledge the generous funding provided by the NIH under the following grant awards: (1) Roadmap grant for a Center for the Multiscale Analysis of Genetic Networks (MAGNet) (U54CA121852), (2) Genetic Network Inference with Combinational Phenotypes (R01CA109755), and (3) In Silico Research Centre of Excellence NCI-caBIG 29XS192. P.S. and A.C. conceived and supervised the project and participated in its computational and experimental design. P.S., H.-S.C, W.-J.C., M.B., and P.G. designed and implemented the computational methods. P.S., X.Y., H.-S.C., and W.-J.C. analyzed data. P.S., X.Y., J.S., and A.C. designed the experimental assays. X.Y., A.I., D.L.-N., and P.R. performed the experiments. P.S., X.Y., H.-S.C., and A.C. wrote the paper.

Received: August 16, 2011
Revised: September 19, 2011
Accepted: September 27, 2011
Published: October 13, 2011

REFERENCES

Arvey, A., Larsson, E., Sander, C., Leslie, C.S., and Marks, D.S. (2010). Target mRNA abundance dilutes microRNA and siRNA activity. Mol. Syst. Biol. *6*, 363.

Barrat, A., Barthelemy, M., and Vespignani, A. (2008). Dynamical processes on complex networks (Cambridge, UK: Cambridge University Press).

Carro, M.S., Lim, W.K., Alvarez, M.J., Bollo, R.J., Zhao, X., Snyder, E.Y., Sulman, E.P., Anne, S.L., Doetsch, F., Colman, H., et al. (2010). The transcriptional network for mesenchymal transformation of brain tumours. Nature *463*, 318–325.

Cesana, M., Cacchiarelli, D., Legnini, I., Santini, T., Sthandier, O., Chinappi, M., Tramontano, A., and Bozzoni, I. (2011). A long noncoding RNA controls muscle differentiation by functioning as a competing endogenous RNA. Cell *147*, this issue, 358–369.

Chatterjee, S., Fasler, M., Büssing, I., and Grosshans, H. (2011). Target-mediated protection of endogenous microRNAs in C. elegans. Dev. Cell *20*, 388–396.

Chi, S.W., Zang, J.B., Mele, A., and Darnell, R.B. (2009). Argonaute HITS-CLIP decodes microRNA-mRNA interaction maps. Nature *460*, 479–486.

Chow, L.M., Endersby, R., Zhu, X., Rankin, S., Qu, C., Zhang, J., Broniscer, A., Ellison, D.W., and Baker, S.J. (2011). Cooperativity within and among Pten, p53, and Rb pathways induces high-grade astrocytoma in adult brain. Cancer Cell *19*, 305–316.

Ebert, M.S., Neilson, J.R., and Sharp, P.A. (2007). MicroRNA sponges: competitive inhibitors of small RNAs in mammalian cells. Nat. Methods *4*, 721–726.

Eiring, A.M., Harb, J.G., Neviani, P., Garton, C., Oaks, J.J., Spizzo, R., Liu, S., Schwind, S., Santhanam, R., Hickey, C.J., et al. (2010). miR-328 functions as an RNA decoy to modulate hnRNP E2 regulation of mRNA translation in leukemic blasts. Cell *140*, 652–665.

Enright, A.J., John, B., Gaul, U., Tuschl, T., Sander, C., and Marks, D.S. (2003). MicroRNA targets in Drosophila. Genome Biol. *5*, R1.

Fisher, R.A. (1925). Statistical methods for research workers (Edinburgh, London: Oliver and Boyd).

Gabriely, G., Yi, M., Narayan, R.S., Niers, J.M., Wurdinger, T., Imitola, J., Ligon, K.L., Kesari, S., Esau, C., Stephens, R.M., et al. (2011). Human glioma growth is controlled by microRNA-10b. Cancer Res. *71*, 3563–3572.

Godlewski, J., Nowicki, M.O., Bronisz, A., Williams, S., Otsuki, A., Nuovo, G., Raychaudhury, A., Newton, H.B., Chiocca, E.A., and Lawler, S. (2008).

Targeting of the Bmi-1 oncogene/stem cell renewal factor by microRNA-128 inhibits glioma proliferation and self-renewal. Cancer Res. *68*, 9125–9130.

Hafner, M., Landthaler, M., Burger, L., Khorshid, M., Hausser, J., Berninger, P., Rothballer, A., Ascano, M., Jr., Jungkamp, A.C., Munschauer, M., et al. (2010). Transcriptome-wide identification of RNA-binding protein and microRNA target sites by PAR-CLIP. Cell *141*, 129–141.

Jeyapalan, Z., Deng, Z., Shatseva, T., Fang, L., He, C., and Yang, B.B. (2011). Expression of CD44 3′-untranslated region regulates endogenous microRNA functions in tumorigenesis and angiogenesis. Nucleic Acids Res. *39*, 3026–3041.

Karreth, F.A., Tay, Y., Perna, D., Ala, U., Tan, S.M., Rust, A.G., DeNicola, G., Webster, K.A., Weiss, D., Perez-Mancera, P.A., et al. (2011). In vivo identification of tumor-suppressive PTEN ceRNAs in an oncogenic BRAF-induced mouse model of melanoma. Cell *147*, this issue, 382–395.

Kanehisa, M., and Goto, S. (2000). KEGG: kyoto encyclopedia of genes and genomes. Nucleic Acids Res. *28*, 27–30.

Kertesz, M., Iovino, N., Unnerstall, U., Gaul, U., and Segal, E. (2007). The role of site accessibility in microRNA target recognition. Nat. Genet. *39*, 1278–1284.

Kim, H., Huang, W., Jiang, X., Pennicooke, B., Park, P.J., and Johnson, M.D. (2010a). Integrative genome analysis reveals an oncomir/oncogene cluster regulating glioblastoma survivorship. Proc. Natl. Acad. Sci. USA *107*, 2183–2188.

Kim, M.S., Oh, J.E., Kim, Y.R., Park, S.W., Kang, M.R., Kim, S.S., Ahn, C.H., Yoo, N.J., and Lee, S.H. (2010b). Somatic mutations and losses of expression of microRNA regulation-related genes AGO2 and TNRC6A in gastric and colorectal cancers. J. Pathol. *221*, 139–146.

Kim, T.M., Huang, W., Park, R., Park, P.J., and Johnson, M.D. (2011). A developmental taxonomy of glioblastoma defined and maintained by MicroRNAs. Cancer Res. *71*, 3387–3399.

Krol, J., Loedige, I., and Filipowicz, W. (2010). The widespread regulation of microRNA biogenesis, function and decay. Nat. Rev. Genet. *11*, 597–610.

Krzywinski, M., Schein, J., Birol, I., Connors, J., Gascoyne, R., Horsman, D., Jones, S.J., and Marra, M.A. (2009). Circos: an information aesthetic for comparative genomics. Genome Res. *19*, 1639–1645.

Kwak, H.J., Kim, Y.J., Chun, K.R., Woo, Y.M., Park, S.J., Jeong, J.A., Jo, S.H., Kim, T.H., Min, H.S., Chae, J.S., et al. (2011). Downregulation of Spry2 by miR-21 triggers malignancy in human gliomas. Oncogene *30*, 2433–2442.

Lee, D.Y., Jeyapalan, Z., Fang, L., Yang, J., Zhang, Y., Yee, A.Y., Li, M., Du, W.W., Shatseva, T., and Yang, B.B. (2010). Expression of versican 3′-untranslated region modulates endogenous microRNA functions. PLoS ONE *5*, e13599.

Lewis, B.P., Burge, C.B., and Bartel, D.P. (2005). Conserved seed pairing, often flanked by adenosines, indicates that thousands of human genes are microRNA targets. Cell *120*, 15–20.

Marioni, J.C., Thorne, N.P., and Tavaré, S. (2006). BioHMM: a heterogeneous hidden Markov model for segmenting array CGH data. Bioinformatics *22*, 1144–1146.

Maslov, S., and Sneppen, K. (2002). Specificity and stability in topology of protein networks. Science *296*, 910–913.

Parsons, D.W., Jones, S., Zhang, X., Lin, J.C., Leary, R.J., Angenendt, P., Mankoo, P., Carter, H., Siu, I.M., Gallia, G.L., et al. (2008). An integrated genomic analysis of human glioblastoma multiforme. Science *321*, 1807–1812.

Poliseno, L., Salmena, L., Zhang, J., Carver, B., Haveman, W.J., and Pandolfi, P.P. (2010). A coding-independent function of gene and pseudogene mRNAs regulates tumour biology. Nature *465*, 1033–1038.

Su, W.L., Kleinhanz, R.R., and Schadt, E.E. (2011). Characterizing the role of miRNAs within gene regulatory networks using integrative genomics techniques. Mol. Syst. Biol. *7*, 490.

Tay, Y., Kats, L., Salmena, L., Weiss, D., Tan, S.M., Ala, U., Karreth, F., Poliseno, L., Provero, P., Di Cunto, F., et al. (2011). Coding-independent regulation of the tumor suppressor PTEN by competing endogenous mRNAs. Cell *147*, this issue, 344–357.

TCGA (Cancer Genome Atlas Research Network). (2008). Comprehensive genomic characterization defines human glioblastoma genes and core pathways. Nature *455*, 1061–1068.

Verhaak, R.G., Hoadley, K.A., Purdom, E., Wang, V., Qi, Y., Wilkerson, M.D., Miller, C.R., Ding, L., Golub, T., Mesirov, J.P., et al; Cancer Genome Atlas Research Network. (2010). Integrated genomic analysis identifies clinically relevant subtypes of glioblastoma characterized by abnormalities in PDGFRA, IDH1, EGFR, and NF1. Cancer Cell *17*, 98–110.

Wang, K., Nemenman, I., Banerjee, N., Margolin, A.A., and Califano, A. (2006). Genome-wide discovery of modulators of transcriptional interactions in human B lymphocytes. RECOMB 2006 also. Lect. Notes Comput. Sci. *3909*, 348–362.

Wang, K., Alvarez, M.J., Bisikirska, B.C., Linding, R., Basso, K., Dalla Favera, R., and Califano, A. (2009a). Dissecting the interface between signaling and transcriptional regulation in human B cells. Pac. Symp. Biocomput., 264–275.

Wang, K., Saito, M., Bisikirska, B.C., Alvarez, M.J., Lim, W.K., Rajbhandari, P., Shen, Q., Nemenman, I., Basso, K., Margolin, A.A., et al. (2009b). Genome-wide identification of post-translational modulators of transcription factor activity in human B cells. Nat. Biotechnol. *27*, 829–839.

Zhao, X., D'Arca, D., Lim, W.K., Brahmachary, M., Carro, M.S., Ludwig, T., Cardo, C.C., Guillemot, F., Aldape, K., Califano, A., et al. (2009). The N-Myc-DLL3 cascade is suppressed by the ubiquitin ligase Huwe1 to inhibit proliferation and promote neurogenesis in the developing brain. Dev. Cell *17*, 210–221.

Zhou, Y., Chen, L., Barlogie, B., Stephens, O., Wu, X., Williams, D.R., Cartron, M.A., van Rhee, F., Nair, B., Waheed, S., et al. (2010). High-risk myeloma is associated with global elevation of miRNAs and overexpression of EIF2C2/AGO2. Proc. Natl. Acad. Sci. USA *107*, 7904–7909.